Microfluid Nanofluid (2004) 1: 62–70
DOI 10.1007/s10404-004-0008-5

RESEARCH PAPER

M. R. Wang · Z. X. Li

Numerical simulations on performance of MEMS-based nozzles at moderate or low temperatures

Received: 13 May 2004 / Accepted: 21 June 2004 / Published online: 14 August 2004

Abstract Performance of microelectromechanical systems (MEMS)-based nozzles at moderate and low temperatures is numerically analyzed using the direct simulation Monte Carlo method. Considering the intermolecular attractive potential caused by low temperature, the generalized soft sphere collision model is introduced. The Larsen–Borgnakke model for the generalized sphere model is used to model the energy exchange between the translational and internal modes. The results for nozzle flows at an initial temperature of 300 K show that the temperature behind the throat is quite low and the intermolecular attractive potential cannot be ignored. Different working conditions in two-dimensional (2D) nozzles are simulated using the present method, including exit pressure, inlet pressure, initial temperature, nozzle geometry, and gas species. The effects on the nozzle performance are analyzed. Simulations on flows in a three-dimensional (3D) low aspect ratio flat nozzle show that the increased surface-to-volume ratio, which leads to high viscosity dissipation, causes a much lower flow characteristic and performance comparing with the 2D case.

Keywords DSMC · Flow field · Generalized soft sphere model · MEMS-based nozzle

Nomenclature

b	miss-distance impact parameter, m
d	collision diameter, m
D_t	throat width, m
E_t	relative translational energy, J
F_t	thruster force, N
I_{sp}	specific impulse, s
k	Boltzmann constant, J/K
Kn_{th}	Knudsen number at throat, defined by averaged values
m	molecular mass, kg
m_r	reduced mass, kg
n	gas number density, m^{-3}
P_{in}	inlet pressure, Pa
P_e	exit pressure, Pa
Re_{th}	Reynolds number at throat, defined by averaged values
T	gas temperature, K
T_*	dimensionless temperature kT/ε
T_w	wall temperature, K
T_{in}	inlet temperature, K
Z_R	rotational relax number
α	soft sphere scattering law
β_j, ω_j	parameters for the GSS model
ε	depth of the potential well, J
δ	dimensionless constant for polarization
μ	gas viscosity, kg/m·s
σ	low-velocity diameter, m
σ_T	total collision cross-section, m^2
ζ_R	rotational degree of freedom
ζ_t	translational degree of freedom
$\Gamma(...)$	gamma function
$\Omega^{(1,1)*}$	integral for the self-diffusion coefficient
$\Omega^{(2,2)*}$	integral for the viscosity

M. R. Wang · Z. X. Li (✉)
Department of Engineering Mechanics,
Tsinghua University, Beijing,
100084 People's Republic of China
E-mail: lizhx@tsinghua.edu.cn
Tel.: +86-10-62772919
Fax: +86-10-62781610

1 Introduction

At present, microelectromechanical system (MEMS)-based "digital micro propulsion" systems have been developed to offer new possibilities of increased orbit and station-keeping or attitude-controlling capabilities at potentially lower cost to small satellites, microsatellites or even nanosatellites (Lewis 1999; Lewis 2000). The thrust must be very low (0.1∼10 mN) for the small mass of a microspacecraft (such as <1 kg). To obtain

these low thrust values, a microscale nozzle and low chamber pressures and temperatures are usually used. This leads to the throat Reynolds number within the range between 10 and 500. As a result of such a low level of Reynolds numbers, the viscous losses are significant in micronozzles.

A number of micronozzles have been developed and the performance has been experimentally studied using mass flow and thrust measurements (Kohler et al. 2002; Kerechanin et al. 2001; Reed et al. 2001; Bayt et al. 1998; Bayt. 1999). The previous performance test for micronozzles indicate that specific impulse efficiencies drop rather dramatically for $Re < 1000$, compared with the ideal situations (Bayt 1999). Therefore, a comprehensive study is indispensable for understanding the special features of viscous flow within such micronozzles and for determining the optimal nozzle geometry, working parameters and gas species, which ensure high performances.

Performance evaluations of micro nozzles have been conducted using the Navier–Stokes (NS) solvers (Bayt 1999; Wang et al. 2001) and the direct simulation Monte Carlo (DSMC) method (Markelov et al. 2001; Hyakutake and Yamamoto 2003; Alexeenko et al. 2002; Alexeenko et al. 2003). It was shown that the uses of the 2D continuum approach led to overpredictions of the specific impulse even for Reynolds numbers $Re \sim 1000$ (Bayt 1999). The standard DSMC of Bird's (1994) or the DSMC-based software, such as the SMILE of Ivanov et al. (1998), were used for micro nozzle performance analysis. Better agreements with the experimental data were found for high-temperature gas flows expanding from micronozzles into a vacuum (Markelov et al. 2001; Hyakutake and Yamamoto 2003; Alexeenko et al. 2002; Alexeenko et al. 2003). In most of the previous simulations, the variable hard sphere (VHS) model (Markelov et al. 2001; Hyakutake and Yamamoto 2003) or the variable soft sphere (VSS) model (Alexeenko et al. 2002; Alexeenko et al. 2003) was used as the intermolecular potential, in which only the repulsive interaction between molecules is considered. However, in actual gases the force between two molecules is not only repulsive at small distances, but also weakly attractive at long distances. The attractive force effect is very weak at high temperatures in a pure gas, and becomes stronger when temperature is low (such as $T < 300$ K). The previous results showed that the transitional temperature near the exit could also be low even if the inlet gas temperature was high in the nozzle exhausting into a vacuum. Therefore, the attractive potential should be considered to improve the nozzle flow simulations.

The first attempt at reproducing the effects of attraction was made by Kuscer (1989) who suggested a total cross that reproduced Sutherland's viscosity formula. Hassan and Hash (1993) and Hash et al. (1994) proposed a generalized hard sphere (GHS) model for a Lennard–Jones fluid. In GHS, the total cross is a function of the gas transitional temperature, while the scattering deflection angle remains the hard sphere value. However, it is hard to fit one set of parameters for a good agreement with the standard values in all transport properties (Kunc et al. 1995). Fan (2002) developed the GHS model. He combined the GHS model and the VSS model, and then proposed a generalized soft sphere (GSS) model. Parameters were determined with least-square fitting and remarkable agreements were found in all transport properties with both theoretical and experimental values at moderate and low temperatures.

In this paper, a detailed performance analysis of two-dimensional (2D) MEMS-based nozzles at moderate or low temperatures is presented using the DSMC method in a GSS model. The influence of the pressure boundary condition, the temperature condition, the nozzle geometry, the throat size, and the gas species on the nozzle performance is examined. The current results are compared with other numerical results (e.g., VSS-DSMC and NS). Finally, the three-dimensional (3D) effect is also discussed.

2 Numerical methods

The DSMC method in the GSS collision model was applied in the present work for the low Reynolds number micronozzle flows at moderate and low temperatures. The GSS model is briefly introduced below.

In the GSS model, the total collision cross-section remains as the GHS rule, which is described by more than one term

$$\frac{\sigma_{\mathrm{T}}}{\sigma^2} = \sum \beta_j \left(\frac{E_{\mathrm{t}}}{\varepsilon}\right)^{-\omega_j} \tag{1}$$

where the parameters β_j and ω_j can be determined from the standard theoretical or experimental transport property data. In general, only two terms on the RHS of Eq. 1 are reserved, so the parameters have to be numerically solved by the least-square fitting.

Because the hard sphere scattering law leads to an unreal ratio of the momentum to viscosity cross-section, the GSS model uses a soft sphere scattering model to calculate the deflection angle

$$\chi = 2 \arccos\left[(b/d)^{1/\alpha}\right] \tag{2}$$

In theory, the coefficients of viscosity and self-diffusion of a simple gas can be expressed in

$$\mu = \frac{5}{16}\left(\frac{\sqrt{\pi m k T}}{\pi \sigma^2 \Omega^{(2,2)^*}}\right) \tag{3}$$

$$D = \frac{3}{16n}\left(\frac{\sqrt{2\pi k T/m_{\mathrm{r}}}}{\pi \sigma^2 \Omega^{(1,1)^*}}\right) \tag{4}$$

where $\Omega^{(1,1)^*}$ and $\Omega^{(2,2)^*}$ in GSS model are

$$\Omega^{(1,1)^*} = \frac{1}{\pi(\alpha+1)} \sum \beta_j \Gamma(3-\omega_j) T_*^{-\omega_j} \tag{5}$$

$$\Omega^{(2,2)*} = \frac{\alpha}{\pi(\alpha+1)(\alpha+2)} \sum \beta_j \Gamma(4-\omega_j) T_*^{-\omega_j} \tag{6}$$

Fan (2002) gave a two-term $\Omega^{(2,2)*}$ fitting the standard data tabulated as functions of T_* from 0.3 to 400 in Hirschfelder et al. (1954). He suggested a set of parameters of GSS as

$$\beta_1 = 3.962 - 0.158\delta \tag{7}$$

$$\beta_2 = 4.558 + 8.660\delta \tag{8}$$

$$\omega_1 = 0.133 \tag{9}$$

$$\omega_2 = 1.25 \tag{10}$$

$$\alpha = 1.5 \tag{11}$$

It was satisfactorily found that the gas properties from the GSS model are in better agreement with the experimental data than other models when using this set of parameters (Fan 2002). In the present paper, they are also employed.

The Larsen–Borgnakke model with discrete rotational energies was used to model the energy exchange between the translational and internal modes. The vibrational energy is ignored because of the moderate and low temperature. As an alternative to the VHS and VSS models, Hash et al. (1994) suggested an averaged relative translational energy in a Hinshelwood type distribution for the generalized molecular model

$$\bar{E}_t = (\zeta_t/2)kT \tag{12}$$

where

$$\zeta_t = 2\left\{2 - \omega_1 + \frac{\omega_1 - \omega_2}{(\alpha_1/\alpha_2)[\Gamma(2-\omega_1)/\Gamma(2-\omega_2)](kT/\varepsilon)^{\omega_2-\omega_1}+1}\right\} \tag{13}$$

With this choice, all computational procedures employed in the VHS or VSS computation can be implemented for the present model. The only additional complexity is that resulting from a calculation of a cell temperature. The probability for the pair selection methodology for rotational relaxation applied in this paper is

$$P_R = (1 + \zeta_R/\zeta_t)/Z_R \tag{14}$$

where Z_R is the rotational relaxation number which is determined by Parker's formula (Hash et al. 1994; Boyd 1993):

$$Z_R = \frac{\left[\sum \alpha_j \left(\frac{T^*}{T}\right)^{\omega_j} \Gamma(2-\omega_1)\right]^{\frac{2-\omega_1}{2}} Z_{R,\infty}}{\sum \alpha_j \left(\frac{T^*}{T}\right)^{\omega_j} \left[\frac{\Gamma(3-\omega_j)}{2} + \frac{2\pi}{3}\Gamma\left(\frac{5}{2}-\omega_j\right)\left(\frac{T^*}{T}\right)^{1/2} + \left(\frac{\pi^2}{4}+2\right)\Gamma(2-\omega_j)\left(\frac{T^*}{T}\right)\right]} \tag{15}$$

The walls are isothermal. The Maxwell model with full momentum and energy accommodation is used for the gas–surface interaction. In this model, the emission of the impinging molecules is not correlated with the pre-impingement state of the molecules. The outgoing velocity is randomly assigned according to a half-range Maxwellian distribution determined by the wall temperature.

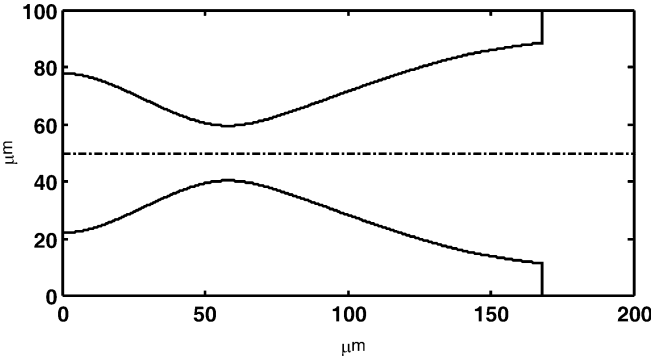

Fig. 1 A Laval micronozzle with the expansion area ratio 3.8 and the throat width 20 μm

The inlet pressure and temperature, as well as the outlet pressure when the outflow is not a vacuum, are specified. The pressure boundary condition of Fang and Liou (2002) is implemented in the present paper.

In current study, the inlet pressure ranges from 1 to 3 atm, the exit pressure from 0.5 atm to a vacuum, the upstream gas temperature from 300 to 1000 K, the expansion area ratio from 1.5 to 3.8, the throat width from 4 to 20 μm, and the gas species varies among N_2, O_2, CO_2, and H_2. Non-uniform rectangular cells with several sub-cells are used and the sub-cell sizes are smaller than the local molecular mean free path. The time step is also smaller than the local averaged collision time. All simulations run on Pentium III 550 MHz processors. The total sample size for each case is greater than 1×10^5, and the running time for each case is more than 100 h.

3 Model comparisons

Before the GSS model is used for simulations and analysis of nozzles, the model applicability is verified firstly. The nozzle performances predicted by the GSS model are compared with those for the VSS model.

The basic nozzle geometry and the computational domain are shown in Fig. 1. The data comes from the experiments of Tang (2003). The standard flow condition (SFC) in this paper is the inlet pressure $P_{in} = 1$ atm, the exit pressure $P_e = 0$ atm (a vacuum), the temperature of the incoming gas and the walls $T = 300$ K, the expansion area ratio is 3.8, and the throat width is 20 μm, for a nitrogen gas flow.

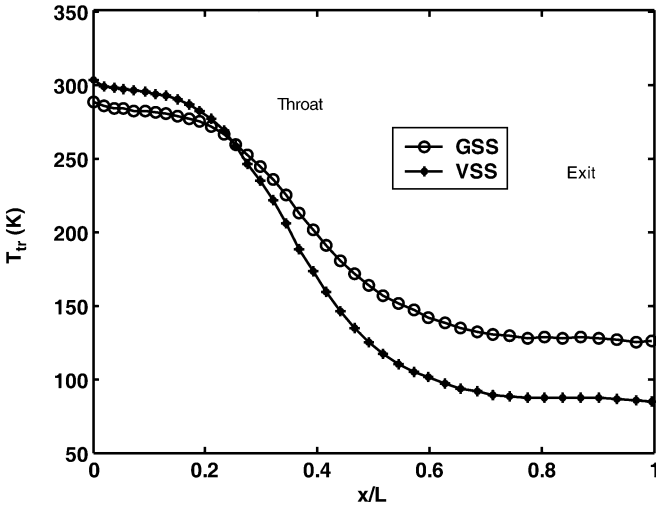

Fig. 2 Transitional temperature along the nozzle centerline for different models ($P_{in} = 1$ atm, P_e is a vacuum, $T_{in} = 300$ K)

Figure 2 shows the comparison of the transitional temperature along the centerline of the nozzle from the GSS-DSMC and the VSS-DSMC under the SFC defined above. The incoming gas temperature is 300 K. The gas exhausts towards the vacuum. It is shown that downstream of the throat, the transitional temperature of the GSS separates clearly from that of the VSS because the temperature is so low that the intermolecular attractive potential cannot be ignored.

Figure 3 shows the Mach number distributions along the centerlines resulting from the GSS-DSMC, VSS-DSMC and the NS solver. The compressible non-slip NS solution is obtained using the commercial code Fluent 6.0 (Fluent Inc., Lebanon, NH, USA) where the low temperature effect on the gas properties (viscosity and thermal conductivity) were taken into consideration. The local Knudsen numbers anywhere in the nozzle are less than 0.016. The figure shows that the

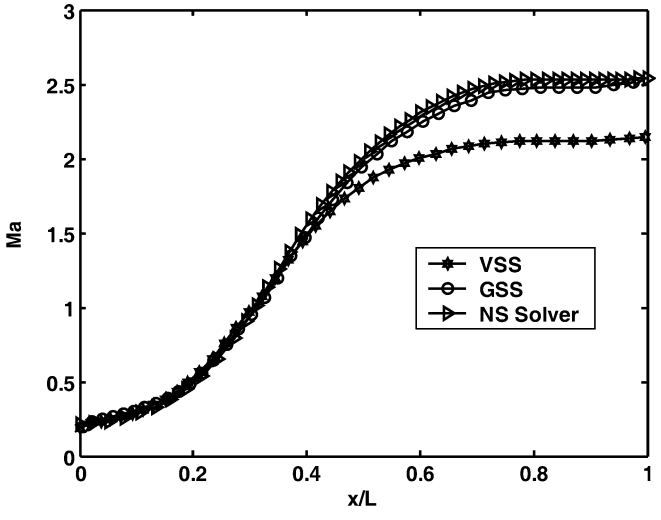

Fig. 3 Mach number along the nozzle centerline for different methods ($Kn_{anywhere} < 0.016$)

Table 1 Nozzle performance calculated in different models for SFC

Performance	Method		
	DSMC(GSS)	DSMC(VSS)	NS(No-slip)
I_{sp} (s)	64.99	65.16	64.00
F_t (mN)	2.47	2.50	2.54

results of the GSS-DSMC agree well with those of the NS solver, while those of the VSS-DSMC differ because of the low temperature. Therefore, it shows that the molecular collision model selection of DSMC has an important effect on the simulations for the moderate and low temperature nozzle flows exhausting into a vacuum.

The nozzle performances calculated by the different models are listed in Table 1 for the standard flow condition. The specific impulse of GSS-DSMC is a little higher than the NS-based result and a little lower than that of VSS-DSMC. However, the thruster force of GSS-DSMC is lower than both the VSS-DSMC and NS methods.

4 Results and discussion

4.1 Exit pressure effects

The exit pressure has a large effect on the nozzle flow. The one-dimensional (1D) theoretical analysis shows that the supersonic flow appears in an ideal Laval nozzle as long as the ratio of outlet pressure to inlet total pressure is less than 0.528. From a 2D analysis for the viscous nozzle flows it is indicated that supersonic conditions remain at the exit only if the pressure ratio is less than a critical value near 0.2 (Hagemann et al. 1998). In this section, nitrogen nozzle flows under different exit pressures are simulated using the GSS-DSMC method. The exit pressures range from 0.5 atm, 0.2 atm and 0.1 atm to 0 atm (a vacuum), where the other flow conditions remain as the SFC. Figure 4 shows the Mach number contours for different exit pressure conditions. From the figure there are three points to note: first, the sonic point is not located at the throat as in the 1D analysis, but behind the throat as a result of the viscosity; second, for the 0.5 atm exit pressure case ($P_e/P_{in} > 0.2$ and $P_e/P_{in} < 0.528$), the supersonic flow exists downstream of the throat but dissipates to subsonic flow rapidly; third, when the exit-to-inlet pressure ratio is much lower than 0.2, the supersonic flow is retained to the exit.

The nozzle performance is greatly affected by the exit pressure. The specific impulse and the thruster force versus the exit pressure are shown in Fig. 5, both of which increase rapidly when the exit pressure is near a vacuum and gently when the exit pressure is far from the vacuum. This might be a reason for the measured nozzle performance being much lower than the predicted value if the exit vacuum condition was not perfectly satisfied.

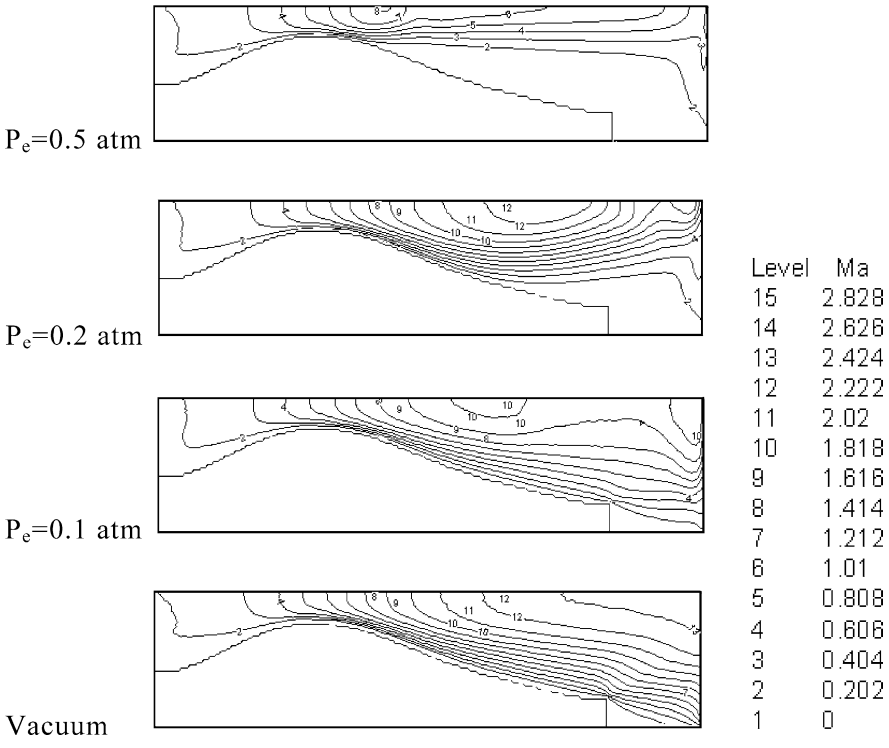

Fig. 4 Mach number fields for $P_{in} = 1$ atm and $T_{in} = 300$ K

4.2 Inlet pressure effects

The inlet pressure effects on the nozzle performance are investigated. The inlet pressure varies from 1 to 3 atm, and the exit pressure is a vacuum. The other conditions are SFC. Table 2 lists the flow characteristics and the nozzle performance under different inlet pressures. The Reynolds numbers at the throat are defined by the averaged macroscopic values of the flow field. It is shown that the thrust force increases nearly proportionally with the inlet pressure; however, the specific impulse increases very little with the inlet pressure.

Table 2 Flow characteristics and the nozzle performance under different inlet pressures

P_0	Re_{th}	F_t (mN)	I_{sp} (s)
1 atm	128.06	2.47	64.99
2 atm	258.05	4.99	65.43
3 atm	387.52	7.52	65.54

Figure 6 shows the dimensionless pressure distributions normalized by the inlet pressures when the inlet pressure varies from 1 to 3 atm. The dimensionless

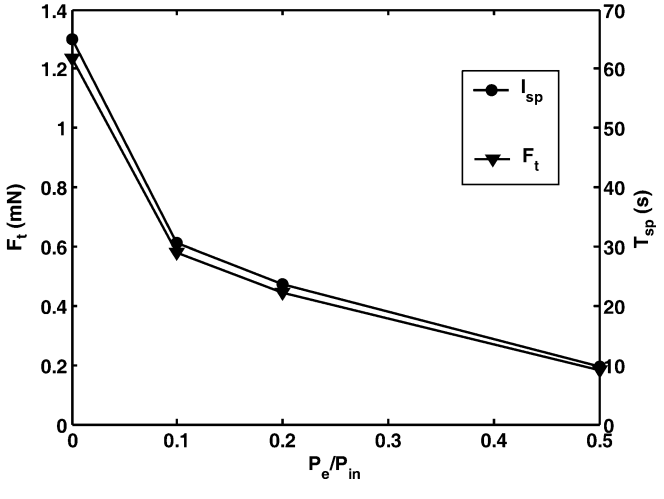

Fig. 5 Thruster force vs. P_e/P_{in} for $T_{in} = 300$ K and $D_t = 20$ μm

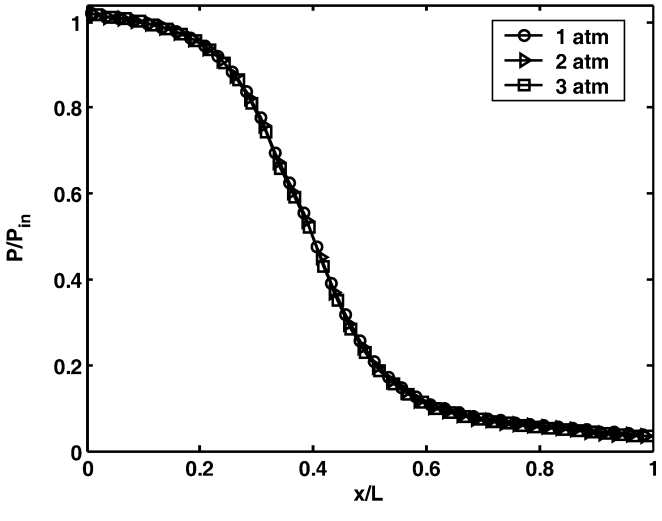

Fig. 6 Normalized pressure along the centerline for different inlet pressures

Table 3 Flow conditions and nozzle performance under different temperature conditions

T	Re_{th}	F_t (mN)	I_{sp} (s)
300 K	128.06	2.47	64.99
400 K	88.72	2.43	74.58
600 K	52.42	2.35	90.22
1000 K	26.52	2.21	113.93

pressure distribution has no relationship with the inlet pressure. The dimensionless pressure at the outlet for each case is about 0.04.

4.3 Temperature effects

In the present simulations, the temperatures of both the incoming gas and the walls are the same. The temperature has an important effect on the nozzle performance, which has been investigated in the literature for high-temperature cases (Alexeenko et al. 2002; Alexeenko et al. 2003; Hash et al. 1994; Tang 2003). Table 3 lists the flow conditions and nozzle performance under different temperature conditions, with an inlet pressure of 1 atm, an outlet at vacuum, an expansion area ratio of 3.8, and a throat width of 20 μm.

The Reynolds number at throat Re_{th} and the thruster force F_t decrease with the temperature, while the specific impulse I_{sp} increases nearly linearly with the temperature. It is shown that the influence of the temperature on the thruster force is not as strong as that on the specific impulse. Especially, when the temperature rises from 300 to 400 K, the specific impulse increases by 14.67%, while the thruster force decreases by 1.43%.

4.4 Geometry effects

The nozzle geometry includes three factors: the throat width, the expansion area ratio, and the channel configuration. First, the throat width effect is considered. The nozzle configuration remains as Fig. 1, with the throat width D_t changing from 20 to 4 μm. Figures 7 and 8 show the velocity and pressure distributions along the channel centerline, where SFC conditions are present. The flow characteristics and the nozzle performance are listed in Table 4.

The decrease in throat width leads to a decrease in Reynolds number, and then a decrease in thruster force. However, the specific impulse is hardly affected.

The configuration and expansion ratio effect on the nozzle performance is investigated. Two new different configuration nozzles are compared with the nozzle shown in Fig. 1. The new nozzle configurations are shown in Fig. 9, in both of which the throat width is 20 μm. Here we name the nozzle in Fig. 1 as nozzle 1, that in Fig. 9a as nozzle 2 and that in Fig. 9b as nozzle 3. Nozzle 2 has an expansion ratio of 1.5. Nozzle 3 has the same expansion ratio as nozzle 1, however, with a different configuration. Table 5 lists the comparisons of the flow characteristics and the nozzle performance.

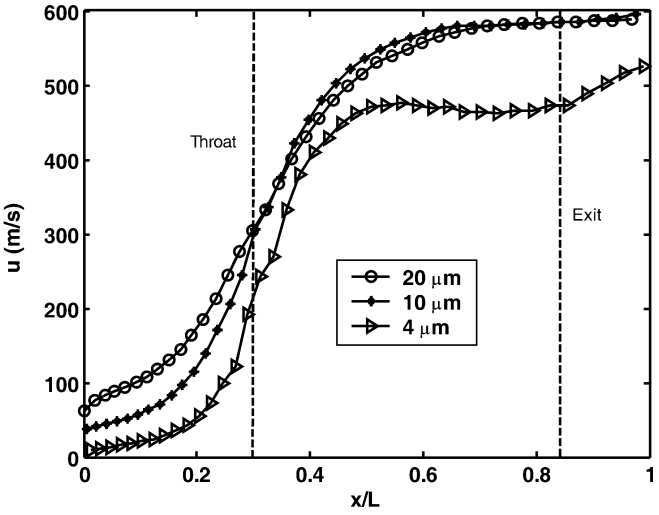

Fig. 7 Velocity along the nozzle centerline for different throat sizes

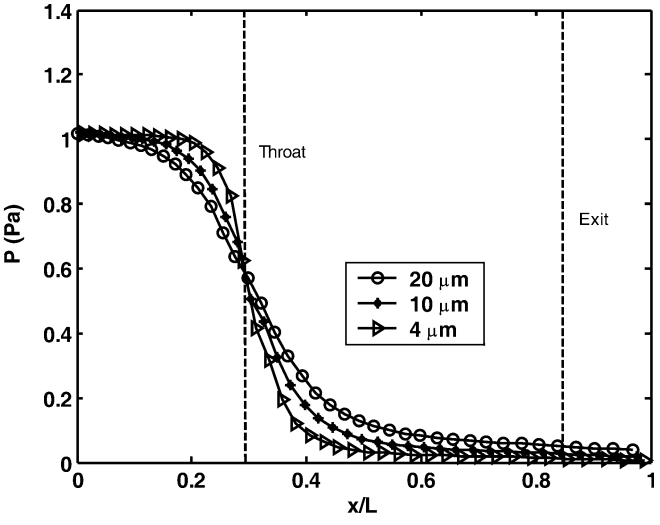

Fig. 8 Normalized pressure along the nozzle centerline for different throat sizes

The pressure and Mach number distributions along the nozzle centerline under SFC are shown in Figs. 10 and 11. In Fig. 10, the inlet Mach numbers are the same as a result of the same inlet pressures and throat sizes for the three cases. The outlet Mach number for nozzle 2 differs from the other two because of its different expansion ratio. The distributions of Mach number

Table 4 Flow characteristics and nozzle performance at different throat width

D_t (μm)	Expansion ratio	Re_{th}	F_t (mN)	I_{sp} (s)
20	3.8	128.06	2.47	64.99
10	6.6	60.27	1.05	64.53
4	15	14.22	0.28	61.10

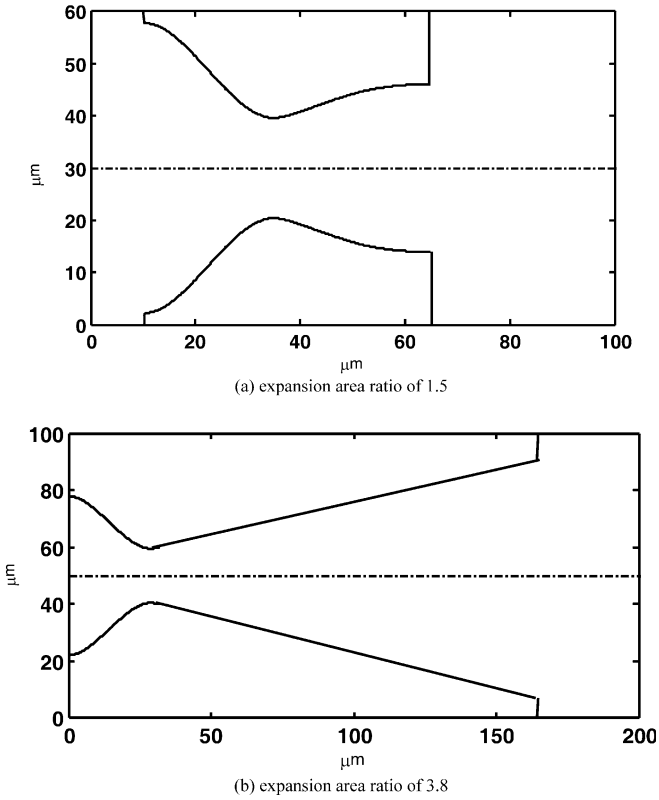

Fig. 9 Two other Laval micronozzle configurations with the throat width of 20 μm. **a** expansion area ratio of 1.5; **b** expansion area ratio of 3.8

differ from each other greatly just because of their different configurations. Figure 11 shows that the inlet-to-outlet pressure ratio is mainly affected by the inlet-to-outlet cross-section ratio.

The results indicate that the nozzle configuration affects the flow characteristics greatly, however, has little effect on the nozzle performance.

4.5 Gas species effects

The nozzle performance simulations are also implemented for different gases species. This paper compares the cases of N_2, O_2, CO_2, and H_2. The gas flows in the geometry 1 nozzle under the conditions of $P_{in} = 1$ atm, $P_e =$ vacuum, $T = 400$ K are calculated. The VSS-DSMC method is used because some parameters in the GSS model are absent for the gases (except for nitrogen). The influence of gas species can be found in Table 6. It shows

Table 5 Flow characteristics and nozzle performance in different nozzle configurations

Configuration	Re_{th}	F_t (mN)	I_{sp} (s)
1	128.06	2.47	64.99
2	354.34	2.53	63.14
3	159.29	2.60	64.59

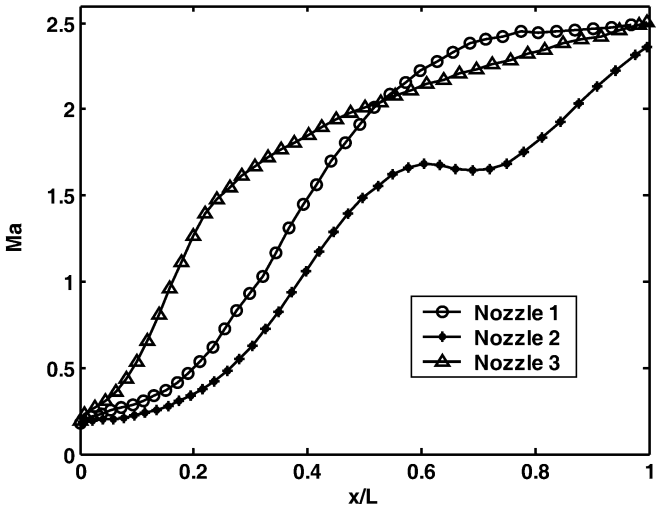

Fig. 10 Mach number along the nozzle centerline for different nozzle configurations

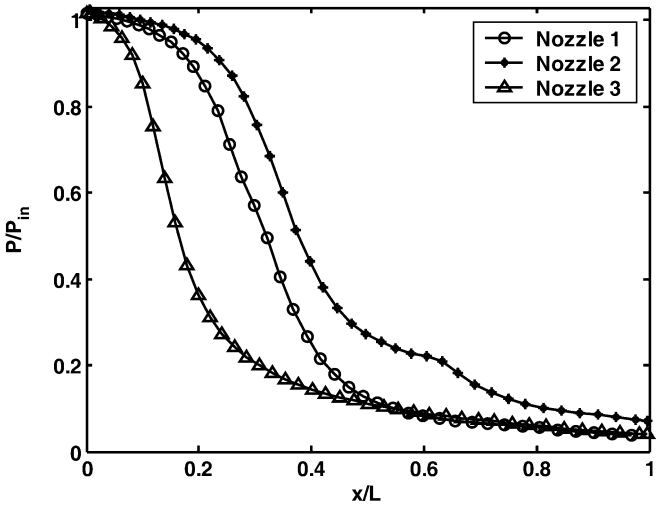

Fig. 11 Normalized pressure along the nozzle centerline for different geometries

that the lightest gas has the best nozzle performance for the micropropulsion, which needs a smaller thruster force and a larger specific impulse.

4.6 3D effects

As opposed to the traditional nozzle, the MEMS-based micronozzles always have a 3D structure instead of an axisymmetric one, as shown in Fig. 12. The surface-to-volume ratio of a flat nozzle is much larger than that of an axisymmetric one, and the surface effects are therefore more pronounced (Alexeenko et al. 2002). Wang and Li (2003) have found that the 2D simplification is reasonable only when the cross aspect ratio is larger than 5 for a straight rectangular cross-section channel.

A low aspect ratio flat nozzle is investigated to analyze the 3D effect on the nozzle performance. In the

Table 6 Flow characteristics and nozzle performance for different gas species

Species	Re_{th}	F_t (mN)	I_{sp} (s)
N_2	92.79	2.58	75.27
O_2	84.94	2.58	70.35
CO_2	132.59	2.68	61.49
H_2	47.70	2.44	275.56

present simulation, the nozzle has a square throat. The 2D nozzle configuration in x–y plane uses the geometry 1, which has a throat width of 20 μm and an expansion area ratio of 3.8. The inlet pressure is 1 atm. The incoming gas temperature is 300 K. The nitrogen gas exhausts into a vacuum. Figure 13 shows the comparisons of Mach number distributions along the centerline between the 2D results and the 3D results at different sections. H is the height of the 3D channel, and h is the distance from the section to the side walls. The Mach numbers obtained from the 3D simulation are much lower than those from the 2D simulation because of increased viscous dissipation. The 3D effects have a lower nozzle performance than predicted by the 2D calculations.

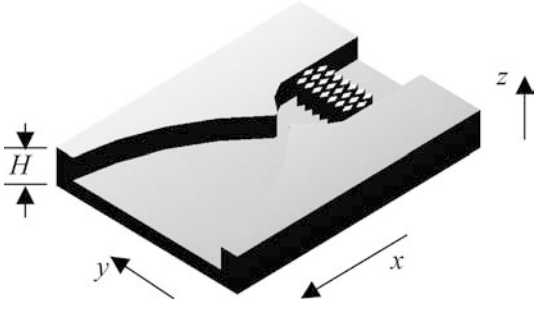

Fig. 12 Schematic of a 3D flat micronozzle

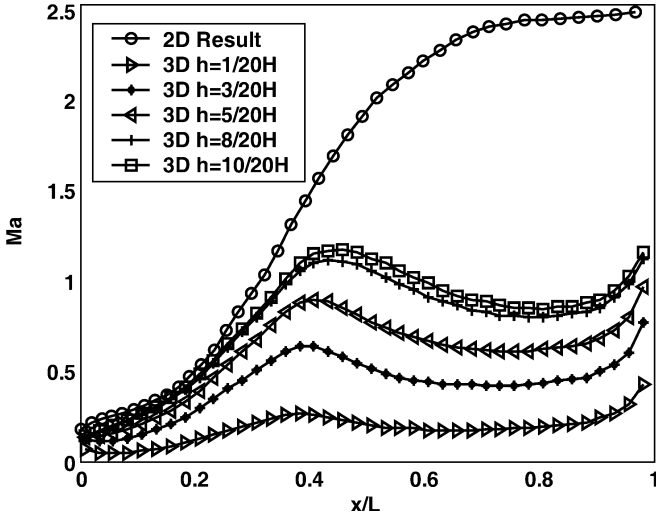

Fig. 13 Mach numbers along centerlines at different sections of the 3D nozzle comparing with the 2D result

5 Concluding remarks

Performance simulations and analyses of MEMS-based nozzles at moderate and low temperatures have been conducted using the DSMC method. The intermolecular attractive potential is considered because of the low temperature and the GSS collision model is introduced. The Larsen–Borgnakke model, which was suggested in the generalized hard sphere model, is used to model the energy exchange between the translational and internal modes. The initial temperature ranges from 300 to 1000 K and the flow Reynolds number at the throat ranges from 14 to 387.

For nozzle flows exhausting into a vacuum at an initial temperature of 300 K, the temperature in the downstream flow of the throat is quite low (far lower than 200 K). The comparisons between the VSS model and the GSS model show that both the temperature and Mach number distributions separate clearly behind the throat. Because the Knudsen number is low (< 0.016), the GSS-DSMC method agrees well with the NS solver in the Mach number distributions along the centerline of the nozzle. The thruster force predicted by GSS-DSMC is a little lower than those by VSS-DSMC and NS solution.

Different working conditions in 2D nozzles are considered. The exit pressure value has a great effect on the nozzle performance and a lower exit pressure leads to a stronger effect. The nozzle thruster force and specific impulse decrease as the exit pressure increases. The inlet pressure affects the thruster force nearly proportionally however has little effect on the specific impulse. A higher initial temperature results in a smaller thruster force and a higher specific impulse. When the throat size is given, the nozzle configuration has a finite effect on the nozzle performance. However, when the nozzle configuration is given the throat size affects the thruster force greatly. Comparisons between different gas species show that a lighter gas can have a higher specific impulse and a smaller thruster force.

3D simulations on a low aspect ratio nozzle flow show that 3D effects cause lower performances compared to the 2D case. The main reason is the increased surface-to-volume ratio, which leads to a high viscous dissipation.

This work gives a solution of performance prediction of MEMS-based nozzles using the DSMC method at moderate and low temperatures. More work should be done to find the optimal nozzle geometries and working conditions in the future.

Acknowledgements The present work was supported by the National Natural Science Foundation of China (Grant No. 59995550–2) and National Key Basic Research and Development Program of China (Grant No. G1999033106).

References

Alexeenko AA, Levin DA, Gimelshein SF (2003) Numerical investigation of physical processes in high-temperature MEMS-based nozzle flows. In: AIP Conf Proc 663(1):760–767

Alexeenko AA, Levin DA, Gimelshein SF, Collins RJ, Markelov GN (2002) Numerical simulation of high-temperature gas flows in a millimeter-scale thruster. J Thermophys Heat Transfer 16:10–16

Bayt RL (1999) Analysis, fabrication and testing of a MEMS-based micropropulsion system. PhD thesis, MIT, Cambridge, MA, USA

Bayt RL, Breuer KS (1998) Viscous effects in supersonic MEMS-fabricated micronozzles. In: Proceedings of the 1998 ASME International Mechanical Engineering Congress and Exposition, Anaheim CA. ASME. New York, pp 117–123

Bird GA (1994) Molecular gas dynamics and the direct simulation of gas flows. Clarendon Press, Oxford

Boyd ID (1993) Temperature dependence of rotational relaxation in shock waves of nitrogen. J Fluid Mech 246:343–360

Fan J (2002) A generalized soft-sphere model for Monte Carlo simulation. Phys Fluids 14:4399–4405

Fang YC, Liou WW (2002) Computations of the flow and heat transfer in microdevices using the DSMC with implicit boundary conditions. J Heat Transfer 124:338–345

Hagemann G, Immich H, Nguyen TV, Dumnov GE (1998) Advanced rocket nozzles. J Propuls Power 14:620–634

Hash DB, Moss JN, Hassan HA (1994) Direct simulation of diatomic gases using the generalized hard sphere model. J Thermophys Heat Transfer 8:758–764

Hassan HA, Hash DB (1993) A generalized hard-sphere model for Monte Carlo simulation. Phys Fluids 5:738–744

Hirschfelder JO, Curtiss CF, Bird RB (1954) Molecular theory of gases and liquid. Wiley, New York

Hyakutake T, Yamamoto K (2003) Numerical simulation of rarefied plume flow exhausting from a small nozzle. In: AIP Conf Proc 663(1): 604–611

Ivanov MS, Markelov GN, Gimelshein SF (1998) Statistical simulation of reactive rarefied flows: numerical approach and applications. AIAA Paper 98–2669

Kerechanin II CW, Samimy M, Kim JH (2001) Effect of nozzle trailing edges on acoustic field of supersonic rectangular jet. AIAA J 39:1065–1070

Kohler J, Bejhed J, Kratz H, Bruhn F, Lindberg U, Hjort K, Stenmark L (2002) A hybrid cold gas microthruster system for spacecraft. Sensors Actuators A 97–98:587–598

Kunc JA, Hash DB, Hassan HA (1995) The GHS interaction model for strong attractive potentials. Phys Fluids 7:1173–1175

Kuscer I (1989) A model for rotational energy exchange in polyatomic gases. Physica A 158:784–800

Lewis DH, Janson JSW, Cohen RB, Antonsson EK (1999) Digital micropropulsion. In: Proceedings of the 12th IEEE International Conference on Micro electro mechanical systems, Orlando, FL, pp 517–522

Lewis DH, Janson JSW, Cohen RB, Antonsson EK (2000) Digital micropropulsion. Sensors Actuators A 80:143–154

Markelov GN, Ivanov MS (2001) Numerical study of 2D/3D micronozzle flows. In: AIP Conference Proceedings 585(1):539–546

Reed BD, Groot W, Dang L (2001) Experimental evaluation of cold flow micronozzles. AIAA Paper 2001-3521

Tang F (2003) Theoretical and experimental study of a silicon microthruster. PhD thesis, Tsinghua University, Beijing

Wang MR, Chen ZJ, Li ZX (2001) Numerical simulation of gas flow in micro Laval nozzles. Piezoelect Acoustoopt 23:207–209 (in Chinese)

Wang MR, Li ZX (2003) Three-dimensional effect of gas flow in micro channels. In: Proceedings of the 12th National Academic Conference on Engineering thermophysics in China, Beijing, pp 673–676 (in Chinese)